PNAS RESEARCH ARTICLE | EARTH, ATMOSPHERIC, AND PLANETARY SCIENCES

Atmospheric heat transport is governed by meridional gradients in surface evaporation in modern-day earth-like climates

Robert Fajber[a,1], Aaron Donohoe[b], Sarah Ragen[c], Kyle C. Armour[a,c], and Paul J. Kushner[d]

Edited by Brian Soden, Rosenstiel School of Marine and Atmospheric Science, University of Miami, Miami, FL; received October 12, 2022; accepted May 10, 2023, by Editorial Board Member Akkihebbal R. Ravishankara

Evaporation adds moisture to the atmosphere, while condensation removes it. Condensation also adds thermal energy to the atmosphere, which must be removed from the atmosphere by radiative cooling. As a result of these two processes, there is a net flow of energy driven by surface evaporation adding energy and radiative cooling removing energy from the atmosphere. Here, we calculate the implied heat transport of this process to find the atmospheric heat transport in balance with the surface evaporation. In modern-day Earth-like climates, evaporation varies strongly between the equator and the poles, while the net radiative cooling in the atmosphere is nearly meridionally uniform, and as a consequence, the heat transport governed by evaporation is similar to the total poleward heat transport of the atmosphere. This analysis is free from cancellations between moist and dry static energy transports, which greatly simplifies the interpretation of atmospheric heat transport and its relationship to the diabatic heating and cooling that governs the atmospheric heat transport. We further demonstrate, using a hierarchy of models, that much of the response of atmospheric heat transport to perturbations, including increasing CO_2 concentrations, can be understood from the distribution of evaporation changes. These findings suggest that meridional gradients in surface evaporation govern atmospheric heat transport and its changes.

water cycle | heat transport | climate dynamics | evaporation | precipitation

Significance

Heat is transported in the atmosphere by the movement of dry air and moisture. This paper demonstrates that, for modern-day Earth-like climates, a large component of the energy transport from dry air comes from condensing water vapor, which converts moisture transport into dry air heat transport. Consequently, the total heat transport by the atmosphere is governed almost exclusively by evaporation, which increases both the water content and total energy of the atmosphere. This perspective on the underlying controls of atmospheric heat transport enables a deeper understanding of the role of the water cycle in atmospheric dynamics and in mediating the response of heat transport to climate change.

The transport of heat through the atmosphere regulates Earth's climate by reducing the equator to pole temperature gradient (1). Fundamentally, this transport exists to balance an energy input to the atmosphere at the equator with an energy loss at the poles (2). In steady state, this connection can be used to calculate the northward meridional heat transport by the atmosphere (AHT) at a given latitude (θ) needed to balance the net energy input into the atmospheric column, Q_{TOTAL}, spatially integrated southward of that latitude (3):

$$\mathrm{AHT}_{\mathrm{TOTAL}}(\theta) = 2\pi a^2 \int_{-\pi/2}^{\theta} Q_{\mathrm{TOTAL}} \cos\theta' d\theta', \quad [1]$$

where Q_{TOTAL} is the difference between the net radiation at the top of the atmosphere (TOA) and the total (radiative plus turbulent) energy flux at the surface. In other words, a positive $\mathrm{AHT}(\theta)$ implies that there is a net gain of atmospheric energy south of that latitude, and the $\mathrm{AHT}_{\mathrm{TOTAL}}$ reflects the northward flow of energy needed to balance the net loss of energy north of that latitude (southward for negative AHT).

$\mathrm{AHT}_{\mathrm{TOTAL}}$ also represents the vertically integrated poleward transport of moist static energy, MSE = $L_v q$ + DSE, where L_v is the latent heat of vaporization, q is the specific humidity, and DSE is the dry static energy, which is the sum of the thermal and gravitational potential energy DSE = $h + \phi$, where h is the enthalpy, and ϕ is the geopotential function. $\mathrm{AHT}_{\mathrm{TOTAL}}$ is frequently separated into a moist component ($\mathrm{AHT}_{\mathrm{MOIST}}$) associated with the vertically and zonally integrated transport of q and a dry component ($\mathrm{AHT}_{\mathrm{DRY}}$) associated with DSE transport:

$$\mathrm{AHT}(\theta) = \mathrm{AHT}_{\mathrm{MOIST}}(\theta) + \mathrm{AHT}_{\mathrm{DRY}}(\theta), \quad [2]$$

which are each calculated analogously to Eq. **1**, but using processes that add and remove water vapor to the atmosphere (for Q_{MOIST}) and processes that heat or cool the atmospheric column (for Q_{DRY}).

Author contributions: R.F. and P.J.K. designed research; R.F. performed research; R.F. contributed new reagents/analytic tools; R.F., A.D., S.R., and K.C.A. analyzed data; and R.F., A.D., S.R., K.C.A., and P.J.K. wrote the paper.

The authors declare no competing interest.

This article is a PNAS Direct Submission. B.S. is a guest editor invited by the Editorial Board.

[1]To whom correspondence may be addressed. Email: rfajber@uw.edu.

This article contains supporting information online at https://www.pnas.org/lookup/suppl/doi:10.1073/pnas.2217202120/-/DCSupplemental.

Published June 13, 2023.

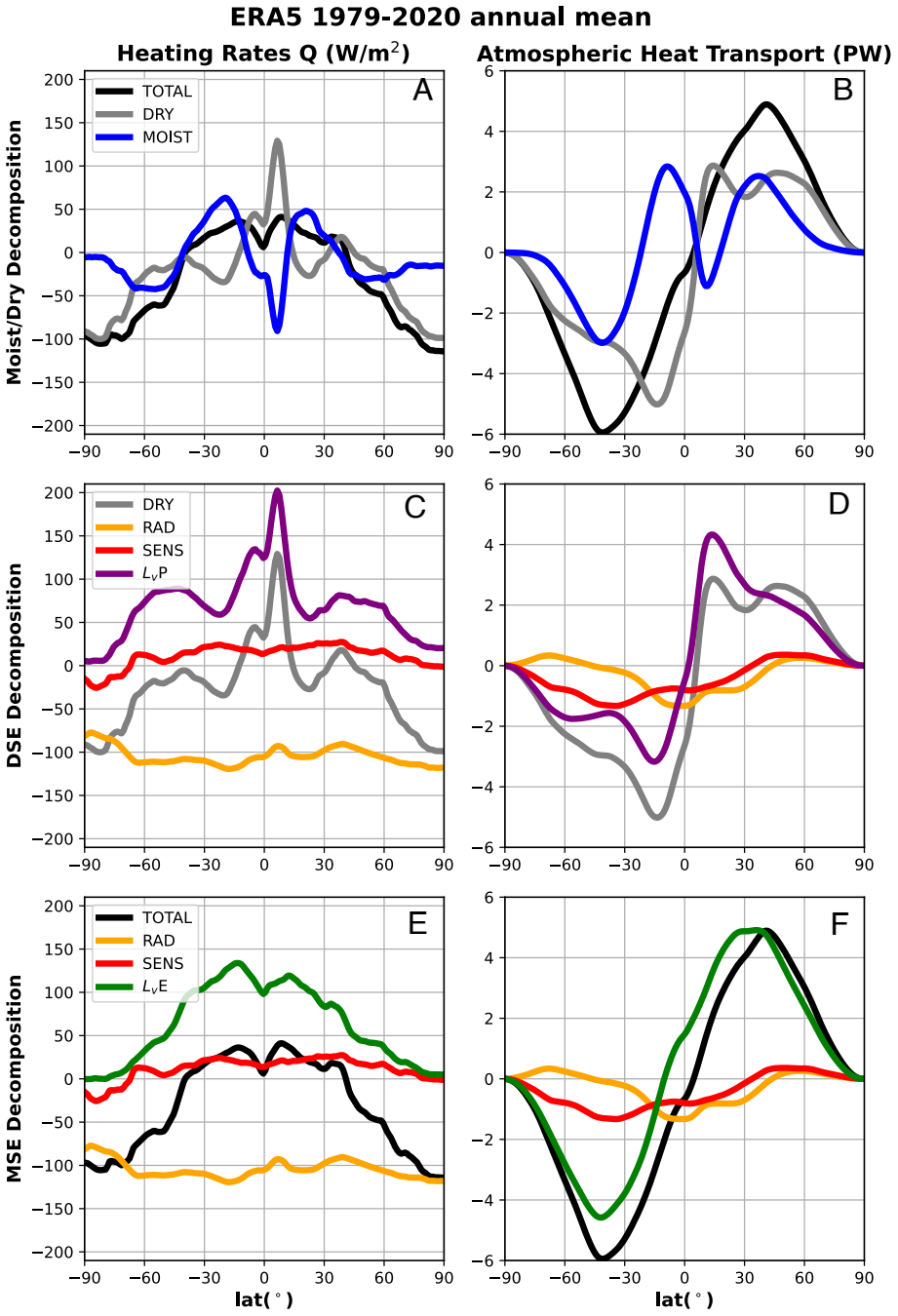

Fig. 1. The column-integrated atmospheric heating rates Q (*A*, *C*, and *E*) and the implied heat transports AHT_{TOTAL} defined by Eq. **5** (*B*, *D*, and *E*) for the standard moist and dry decomposition defined by Eq. **2** (*A* and *B*), the decomposition of the DSE defined by Eq. **4** (*C* and *D*), and the decomposition of MSE defined by Eq. **6** (*E* and *F*).

AHT_{TOTAL}, AHT_{MOIST}, and AHT_{DRY}, evaluated from Q_{DRY} and Q_{MOIST} in the ERA5 reanalysis dataset (4), are shown in Fig. 1. The global mean of Q_{MOIST} and Q_{DRY} are physically constrained to be zero in equilibrium to satisfy separate atmospheric moisture and energy budgets, which is part of the motivation for dividing Q_{TOTAL} into Q_{MOIST} and Q_{DRY}.*

Q_{TOTAL} (black line in Fig. 1 *A* and *E*) is broadly positive over the tropics and subtropics where the atmosphere gains energy through large turbulent fluxes from the surface (red and green lines in Fig. 1*E*) and broadly negative over the midlatitudes and poles where radiative cooling (orange line in Fig. 1*E*) dominates. There is substantially more meridional structure in Q_{MOIST} and Q_{DRY} separately. Q_{MOIST} (blue line in Fig. 1*A*) is the difference between evaporation (green line in Fig. 1*E*) and precipitation (purple line in Fig. 1*C*). The dynamics of the atmosphere diverge water vapor from the subtropics where evaporation is larger than precipitation (Q_{MOIST} is positive) and supply the moisture needed to the tropics and extratropics to sustain greater precipitation than evaporation. In the tropics, the dynamical transport is largely accomplished by the Hadley cell, while in the extratropics, a complex mix of stationary and transient eddies move water vapor poleward (5, 6). Q_{DRY} (gray line in Fig. 1 *A* and *C*) is strongly positive in the tropics, near

*In general, reanalysis products do not satisfy these budgets; therefore, here we remove the global means of Q_{MOIST} and Q_{DRY} separately to enforce these constraints, *Materials and Methods* for details.

zero or slightly positive in the midlatitude storm tracks because of strong condensation (equivalent to the purple line in Fig. 1*C*), and negative in the subtropics and extratropics where the radiative processes cool the atmosphere more strongly (orange line in Fig. 1*C*) (2) than condensation. These processes will be discussed more quantitatively in the next section.

Whereas $\mathrm{AHT_{TOTAL}}$ is a smoothly varying function of latitude, representing a seamless energy transport from the equator to the pole (7, 8), $\mathrm{AHT_{MOIST}}$ and $\mathrm{AHT_{DRY}}$ have strong, compensating latitudinal variations. In the tropics, an equatorward $\mathrm{AHT_{MOIST}}$ in the lower branch of the Hadley cell is counteracted by a larger magnitude poleward $\mathrm{AHT_{DRY}}$ in the upper branch of the Hadley cell. In the midlatitudes, there is complementary poleward $\mathrm{AHT_{MOIST}}$ and $\mathrm{AHT_{DRY}}$ of comparable magnitude by the midlatitude eddies. In the polar latitudes, $\mathrm{AHT_{MOIST}}$ nearly vanishes. The spatial structures of $\mathrm{Q_{MOIST}}$ and $\mathrm{Q_{DRY}}$ are imprinted on $\mathrm{AHT_{MOIST}}$ and $\mathrm{AHT_{DRY}}$, most notably in the tropics where strong precipitation creates a deficit in $\mathrm{Q_{MOIST}}$, which causes $\mathrm{AHT_{MOIST}}$ to switch sign. How the $\mathrm{AHT_{MOIST}}$ and $\mathrm{AHT_{DRY}}$ interact to sum to a smooth function of latitude, in both the climatology and in perturbations under climate forcing, is a primary focus of this paper.

Numerous studies have sought to understand the partitioning of $\mathrm{AHT_{TOTAL}}$ into $\mathrm{AHT_{MOIST}}$ and $\mathrm{AHT_{DRY}}$ in observations, e.g., refs. 8–11, idealized circulation models, e.g., refs. 12–15, and realistic global climate models, e.g., refs. 16–18, as well for the response of each to global climate change, e.g., refs. 3, 19, and 20 and solar climate forcing, e.g., refs. 21, 22. However, this understanding is complicated by the strong compensations in latitudinal variations between $\mathrm{AHT_{MOIST}}$ and $\mathrm{AHT_{DRY}}$ (Fig. 1*B*). In the next section, we demonstrate how this compensation arises from condensation of water vapor, which removes latent energy and adds thermal thermal energy in equal and opposite amounts, creating opposite responses in $\mathrm{AHT_{MOIST}}$ and $\mathrm{AHT_{DRY}}$. Furthermore, we will show that these compensating components can be combined into a single component using the distribution of evaporation at the surface, and which is nearly equal to the total AHT. This analysis suggests that the meridional gradients of evaporation play a primary role in governing AHT—a hypothesis that we explore in the remainder of the paper using a hierarchy of climate model simulations.

Isolating the Atmospheric Heat Transport Governed by Evaporation

To understand the connections between $\mathrm{AHT_{MOIST}}$ and $\mathrm{AHT_{DRY}}$, we decompose $\mathrm{Q_{MOIST}}$ and $\mathrm{Q_{DRY}}$ into different physical processes:

$$\mathrm{AHT_{MOIST}}(\theta) = 2\pi a^2 \int_{-\pi/2}^{\theta} \underbrace{L_v(E-P)}_{Q_{\mathrm{MOIST}}} \cos\theta' d\theta', \qquad [3]$$

where E is the evaporation and P is the precipitation, and

$$\mathrm{AHT_{DRY}}(\theta) = 2\pi a^2 \int_{-\pi/2}^{\theta} \left(\underbrace{\overbrace{L_v P}^{Q_{\mathrm{COND}}} + Q_{\mathrm{SENS}} + Q_{\mathrm{RAD}}}_{Q_{\mathrm{DRY}}} \right) \cos\theta' d\theta', \qquad [4]$$

where $\mathrm{Q_{SENS}}$ is the sensible flux from the surface, and Q_{RAD} is the difference between the top of atmosphere and surface radiative fluxes, e.g., refs. 10 and 23. We note that Q_{RAD} is the radiation absorbed only in the atmospheric column, which is distinct from the radiation at the top of the atmosphere (shown separately in *SI Appendix*, Fig. S1). In Eq. **4**, we equate condensational heating of the atmospheric column, $\mathrm{Q_{COND}}$, with the latent heat of falling precipitation, which enables us to evaluate $\mathrm{AHT_{DRY}}$ from two-dimensional inputs.

Precipitation occurs in the equations for both the $\mathrm{AHT_{MOIST}}$ (Eq. **3**) and $\mathrm{AHT_{DRY}}$ (Eq. **4**) with opposing signs. Physically, this occurs because condensation removes water vapor, creating precipitation and reducing $\mathrm{AHT_{MOIST}}$, and also adds thermal energy to the atmosphere, increasing DSE and $\mathrm{AHT_{DRY}}$. In this sense, the precipitation facilitates a hand-off from $\mathrm{AHT_{MOIST}}$ to $\mathrm{AHT_{DRY}}$, while leaving $\mathrm{AHT_{TOTAL}}$ the same. This hand-off looks different in the tropics and the extratropics; in the tropics, it occurs between the upper and lower branches of the Hadley cell which move in opposite directions (8), whereas in the extratropics, it occurs in the eddying circulation, so the transport is in the same direction (5, 6).

In order to isolate the effect of precipitation on $\mathrm{AHT_{DRY}}$, we separate the physical processes on the right-hand side of Eq. **4** and find an implied heat transport for each. For the atmosphere to be in steady state, the global mean of Q_{TOTAL} must be zero (otherwise the atmosphere would be gaining or losing energy), which implies that $\mathrm{AHT_{TOTAL}}$ depends only on gradients in $\mathrm{Q_{TOTAL}}$. The implied heat transport for any given physical process can be found by first removing the global mean and then integrating the meridional anomalies. For example, we define the implied $\mathrm{AHT_{TOTAL}}$ of precipitation (AHT_{L_vP}) as

$$\mathrm{AHT}_{L_vP}(\theta) \equiv 2\pi a^2 \int_{-\pi/2}^{\theta} L_v P^* \cos\theta' d\theta', \qquad [5]$$

where $(\cdot)^*$ indicates the anomalies from a global average. The implied transports for surface sensible heat flux ($\mathrm{AHT_{SENS}}$) and radiative heating of the atmospheric column ($\mathrm{AHT_{RAD}}$) are calculated by replacing $\mathrm{L_vP^*}$ with $\mathrm{Q^*_{SENS}}$ and $\mathrm{Q^*_{RAD}}$, respectively, in Eq. **5**. Eq. **5** implies that it is the processes with the largest meridional gradients, and not the largest global means, that contribute the most to AHT.

Removal of the global mean from each term constrains the implied AHT of each energetic process to equal zero at both poles. Physically, for a process which is not zero in steady state, removing a global mean is equivalent to balancing that term with a globally uniform term of the opposite sign. For example, in the case of precipitation, L_vP^* is the meridional gradient created by balancing the condensational heating with a globally uniform cooling; the implied AHT is the heat transport needed to redistribute the heat produced by regions with a surplus of condensation (L_vP^* is positive) to regions with a deficit (L_vP^* is negative).

The physical processes that make up $\mathrm{Q_{DRY}}$ are shown in Fig. 1*C*. The dominant global mean balance is between atmospheric warming by L_vP and atmospheric cooling by $\mathrm{Q_{RAD}}$. However, L_vP has much larger spatial gradients than either $\mathrm{Q_{RAD}}$ or $\mathrm{Q_{SENS}}$. As a consequence of Eq. **5**, $\mathrm{AHT_{DRY}}$ is dominated by AHT_{L_vP}, especially in the northern hemisphere. In other words, the largest component of $\mathrm{AHT_{DRY}}$ is the redistribution of DSE needed to balance the excess condensational heating in the tropics which is associated with intense tropical precipitation. Thus, despite the fact that $\mathrm{AHT_{DRY}}$ is a transport of dry air, it is largely determined by moist atmospheric processes which control condensational heating.

Since AHT_{L_vP} is such a large component of $\mathrm{AHT_{DRY}}$, it is useful to combine it with $\mathrm{AHT_{MOIST}}$ and calculate a net heat

transport associated with evaporation. This can be done by adding Eqs. **3** and **4** to calculate AHT_{TOTAL} in a new way:

$$AHT_{TOTAL} = 2\pi a^2 \int_{-\pi/2}^{\theta} \left(\underbrace{L_v E + Q_{SENS} + Q_{RAD}}_{Q_{TOTAL}} \right) \cos\theta' d\theta'. \quad [6]$$

In this recasting of AHT_{TOTAL}, the term LvE represents the implied heat transport due to evaporation (AHT_{LvE}), which can be calculated analogously to AHT_{LvP}. A key feature of AHT_{L_vE} is that it isolates the heat transport from evaporation from AHT_{SENS} and AHT_{RAD}, which appear in AHT_{DRY} and AHT_{TOTAL}. Since the gradients of L_vE are much larger than the gradients in Q_{SENS} and Q_{RAD}, AHT_{L_vE} is much larger than AHT_{SENS} and AHT_{RAD} (Fig. 1 *E* and *F*).

Since $E = (E - P) + P$, $AHT_{LvE} = AHT_{MOIST} + AHT_{LvP}$. In other words, AHT_{L_vE} combines two different physical types of heat transport; AHT_{MOIST} is a transport of water vapor in the atmosphere, while AHT_{LvP} is a transport of heat created by condensation by dry air. The conversion between the two components is determined by the location of condensation (precipitation), which converts latent energy to DSE, and hence converts AHT_{MOIST} to AHT_{LvP}. Since both components involved in this conversion are included in the MSE budget, condensation plays no role in AHT_{TOTAL} (24) and does not appear in Eq. **6**. Physically, this can be rationalized by comparing the moist processes in Eqs. **3**, **4**, and **6**. Evaporation adds moisture and MSE to the atmosphere, and precipitation (condensation) removes moisture and adds a compensating amount of DSE to the atmosphere. Therefore, the distribution of evaporation determines where MSE is added to the atmosphere and thus AHT_{LvE} and AHT_{TOTAL}, whereas the distribution of precipitation (condensation) determines how the AHT is partitioned between AHT_{MOIST} and AHT_{LvP}.

Comparing Fig. 1*F* and Fig. 1*B*, the complex latitudinal interplay between AHT_{MOIST} and AHT_{DRY} has been replaced by the smooth AHT_{L_vE}, explaining why AHT_{TOTAL} varies smoothly (c.f. the green line representing AHT_{L_vE} and the black line representing AHT_{TOTAL} in Fig. 1*F*). This simpler picture emerges because the compensating effects of precipitation on AHT_{MOIST} Eq. **3** and AHT_{DRY} Eq. **4** have been removed in Eq. **6**. Note that the nature of how the compensation takes place is irrelevant; the compensation in the tropics composed of two countermoving transports and the compensation in the poleward eddying circulation have both been removed. This is because the compensation is related to a fundamental energetic relationship and not dependent on the nature of the circulation.

This perspective explains the compensation of AHT_{MOIST} and AHT_{DRY} in the tropics. Near the equator, the surface branch of the Hadley cell creates a large equatorward AHT_{MOIST}, but the condensation in the upward branch creates a large poleward AHT_{L_vP}, which nearly compensates AHT_{MOIST} leaving a relatively small AHT_{TOTAL}. The small AHT_{TOTAL} can be seen to result from relatively small meridional gradients in evaporation in the deep tropics. The importance of AHT_{L_vE} explains why AHT_{TOTAL} in the Hadley cycle is strongly affected by evaporation (25), while changing atmospheric moisture content creates compensating changes in AHT_{MOIST} and AHT_{DRY} (13). At the edge of the Hadley cell, the redistribution of DSE to balance tropical latent heating is accomplished through a complex mixture of mean and eddy transport (8, 18), but ultimately exists to move the heat produced by the condensation further poleward.

In the mid-latitudes, the sharp transition between AHT_{MOIST} and AHT_{DRY} is caused by a similar compensation near the storm tracks where strong condensation heating occurs (2). Since condensation does not change AHT_{L_vE}, it does not show the same sharp transition. Additionally, while AHT_{MOIST} is near zero at polar latitudes—due to the limited capacity of the atmosphere to hold water vapor at low temperature (19)—AHT_{L_vE} has relatively large values near the poles. This result indicates that a substantial portion of the meridional pattern of atmospheric heating governing AHT_{DRY} comes from condensational heating, even at polar latitudes far away from regions of strong condensational heating (26).

In summary, we have decomposed AHT_{TOTAL} into transports implied by key physical processes that add and remove energy from the atmospheric column. Instead of the usual dry and moist decomposition, the decomposition used here demonstrates that AHT_{TOTAL} is primarily in balance with the meridional gradient in evaporation. Normally, gradients in evaporation are not associated with the total heat flux. This is because the heat transport implied by the gradients in evaporation includes both a direct transport of moisture (AHT_{Lv_E}) and a transport of DSE (AHT_{DRY}), which compensate each other. Since evaporation is largely controlled by the Clausius–Clapeyron relation (27), it is much larger in the tropics than at the poles, and thus, there is a large equator-to-pole gradient in evaporation (28). The importance of AHT_{L_vE} to AHT_{TOTAL} suggests that AHT_{TOTAL} exists, in large part, to balance the meridional gradient of evaporation.

Model Evidence Demonstrates a Causal Link Between Evaporation and Atmospheric Heat Transport

Through the arguments above, the strong similarity between AHT_{L_vE} and AHT_{TOTAL} suggests that the meridional distribution of evaporation is causally linked to the total atmospheric heat transport. In this section, we use multiple lines of evidence to show that this is the case: first, by tracking the heat added to the atmosphere using passive tracers; second, by showing that changes in surface boundary condition (distribution of land and ocean heat transport) are coupled to the AHT through changes in evaporation; third, by showing that the reductions in evaporation (either by changing the surface flux parameterization or by covering the surface with sea ice) lead to decreases in AHT; and fourth, by showing that in response to increased CO_2, AHT increases through an increase in evaporation. In all cases, changes in the meridional gradient in surface evaporation provide an accurate prediction for changes in AHT_{TOTAL}. Taken together, these experiments demonstrate that changes to surface evaporation result in changes to AHT and that understanding the distribution of surface evaporation is critical to understanding AHT.

A. Passive Tracer Transport Follows the Energy Added by Evaporation. Following the methods of ref. 26, we include "heat tags" in a simplified atmospheric aquaplanet model[†] by adding a passive tracer whenever condensation takes place and removing this tracer wherever cooling takes place. This allows us to track how the DSE generated by condensation at each

[†]The ISCA model (29), using a gray radiation scheme with parameterized water vapor window; see *Materials and Methods* for further details.

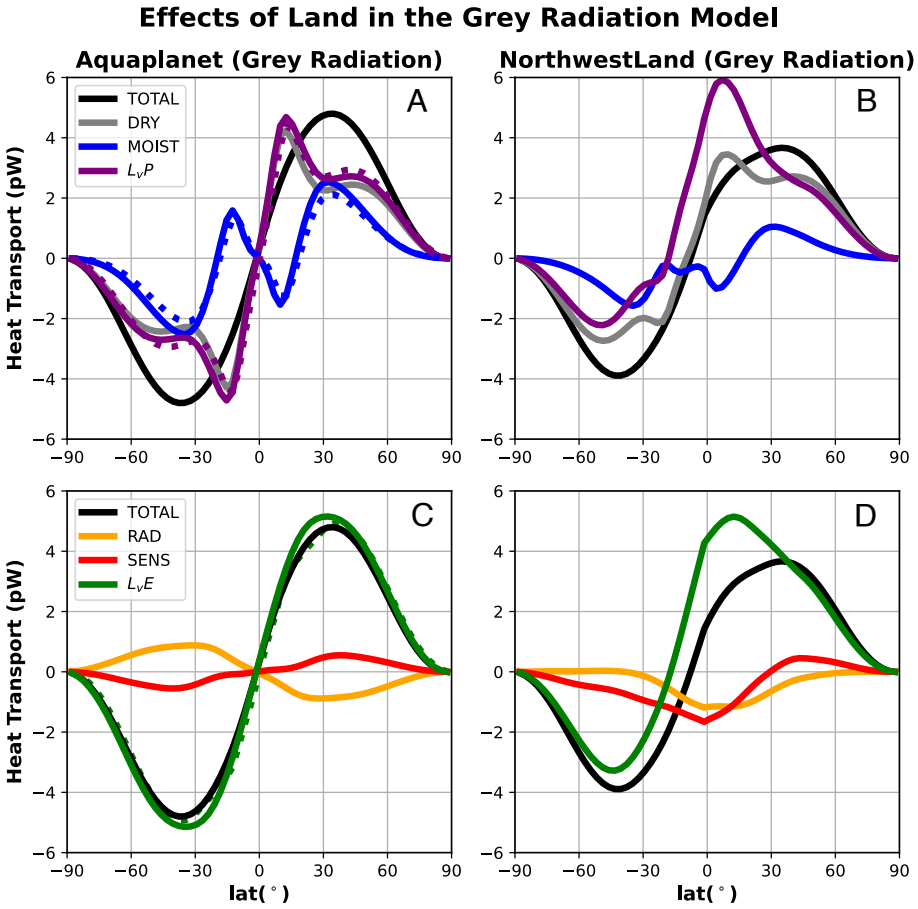

Fig. 2. Implied heat transports for the Aquaplanet (*A* and *C*) and the NorthwestLand experiment (*B* and *D*), showing the moist, dry decomposition and AHT_{L_vP} (*A* and *B*) and the MSE decomposition (*C* and *D*).

latitude is transported (or dissipated radiatively) and calculate an independent estimate of AHT_{L_vP} (dashed purple line in Fig. 2*A*). Similarly, we independently diagnose AHT_{MOIST} from the vertical and zonal integral of the product of meridional winds and L_vq (dashed blue line in Fig. 2*A*). These "tagging" and dynamics-based calculations of AHT_{L_vP} and AHT_{MOIST}, respectively, can be combined to form an independent calculation of AHT_{L_vE}, which is shown in the dashed green line of Fig. 2*C*.

The implied heat transports calculated from Eq. **5** applied to the aquaplanet model output fields (evaporation and precipitation) are shown by solid lines alongside the "tagged" transports in Fig. 2 *A* and *C*. There is good agreement between the two independent calculations of the implied heat transports resulting from each energetic process. This result indicates that our method of calculating the implied AHT needed to balance the meridional energy imbalances into the atmosphere matches the dynamically calculated heat transport, which allows us to interpret the implied transports as the actual heat transports. Also, the heat tags demonstrate that the majority of AHT can be directly traced to evaporation, with a significant DSE component that comes from condensation. Importantly, because heat tags are computationally demanding, the implied AHT method allows us to diagnose the heat transport components from standard surface and TOA fluxes. This also allows us to extend our analysis to models which do not include these tagged tracers, as well as to observations.

We hypothesize that the reason our implied flux method matches the heat tagging method so well is that the dominant energy balance in the atmosphere is between a term with strong meridional gradients (evaporation) and a term with weak meridional gradients (radiation). In AHT_{L_vE}, we have removed the global mean, effectively balancing the evaporation with a globally uniform cooling; however, this is similar to the actual radiation term, so the implied heat transport will be similar to the heat tag calculation which uses the actual distribution of atmospheric cooling. This balance is similar in both the idealized model and reanalysis, providing evidence that our interpretation of the implied reanalysis heat transport as the actual heat transport is well justified.

B. The Response of the Atmospheric Heat Transport to Different Surface Boundary Conditions Is Mediated through Evaporation. A key difference between the idealized model and the reanalysis data is the nature of the interhemispheric transport. The idealized model is hemispherically symmetric, and there is strong compensation between AHT_{SENS} and AHT_{RAD}. In the reanalysis data, there is southward AHT_{TOTAL} at the equator, with a northward AHT_{L_vE} opposed by southward AHT_{SENS} and AHT_{RAD}.

To examine the role of evaporation in creating the hemispheric asymmetry, we consider the "NorthwestLand" model,[‡] which has a landmass in the northern hemisphere. Simply adding this landmass—without the inclusion of clouds, poleward ocean heat

[‡]Originally reported on in ref. 31; *Materials and Methods* for further details. The model climatology is shown in *SI Appendix*, Fig. S2.

transport (OHT), or sea ice—creates a hemispheric asymmetry with a northward AHT_{L_vE} opposed by southward AHT_{SENS} and AHT_{RAD} (Fig. 2*D*). Similar to ERA5 at the equator, the Northwestland model has a northward AHT_{TOTAL} due to the lack of ocean heat transport, which is thought to create southward AHT_{TOTAL} at the equator in nature (32). Over the land, the limited water availability decreases L_vE, so the larger ocean surface in the southern hemisphere causes a northward AHT_{L_vE} across the equator. The Q_{SENS} and Q_{RAD} over land are more positive, so there are compensating AHT_{SENS} and AHT_{RAD} southward at the equator.

We further demonstrate this point by recalculating AHT_{L_vE}, AHT_{SENS} and AHT_{RAD} for a modified set of fluxes created by replacing the surface fluxes over land with the ocean mean of surface fluxes at the same latitude (*SI Appendix*, Fig. S3 *A–C*). This removes almost all of the hemispheric asymmetry, demonstrating that the majority of the interhemispheric heat transport is caused by differences in Q_{TOTAL} above land and ocean, and not to differences in mean climate (e.g., difference in temperature or winds) between the two hemispheres. This approach can be applied to the ERA5 reanalysis (*SI Appendix*, Fig. S3 *D–F*), which shows remarkably consistent results with the idealized model, emphasizing the role that the distribution of land plays in causing the hemispheric asymmetry.

We next investigate the effects of OHT, which substantially modifies the climate (33, 34), and AHT (15, 34), since AHT and OHT compensate each other. This is because while the total heat transport is driven by the top of atmosphere radiation, the partitioning between the OHT and AHT is set by the surface energy balance (10, 18). Thus, changing the OHT will result in changes to the surface fluxes and thus change the AHT (34). Of particular interest in this study is the role of the wind-driven subtropical ocean cells, which partition the total poleward heat transport between the atmosphere and ocean in the tropics (35–38) where evaporation is the strongest.

To investigate how the AHT is coupled to OHT, we introduce a poleward OHT in the subtropics (mimicking that of the wind-driven subtropical cells) of the slab ocean aquaplanet model, accomplished by adding a prescribed pattern of ocean heating and cooling. In response to this OHT, poleward AHT_{TOTAL} decreases, accomplished by compensating decreases in tropical AHT_{MOIST} and AHT_{DRY} (Fig. 3*A*). Again, calculating AHT_{L_vE} removes the compensation between AHT_{MOIST} and AHT_{DRY}; the change in AHT_{TOTAL} is almost exactly equal to AHT_{L_vE} (Fig. 3*C*). In physical terms, the increase in OHT is communicated to the atmosphere through reduction in subtropical evaporation, which reduces the amount of energy for the atmosphere to transport poleward.

C. Reducing Evaporation Reduces Atmospheric Heat Transport. To further evaluate the role evaporation plays in governing atmospheric heat transport, we next perform an experiment in which we divide the coefficient controlling the magnitude of surface evaporation in half. The tropics cool in this simulation due to atmospheric drying; the drier atmosphere is more longwave transparent (due to parameterized water vapor feedback included in the gray radiation model), and this allows longwave radiation to efficiently be emitted to space (a cooling tendency). Global mean evaporation is reduced by only 30.% (*SI Appendix*, Fig. S4) because of changes in the air–sea temperature gradient, which create compensating changes to the sensible and longwave surface heat fluxes.

Reducing evaporation causes a reduction in AHT_{TOTAL}. Similar to the simulation with prescribed OHT, the reduced AHT_{TOTAL} results from compensating changes in AHT_{MOIST} and AHT_{DRY} (Fig. 3*B*). Analysis of AHT_{L_vE} simplifies the analysis of changes in AHT_{TOTAL} under reduced evaporation. Instead of the intricate patterns of compensation between AHT_{MOIST} and AHT_{DRY}, changes in AHT are due entirely to a reduction in AHT_{L_vE} that smoothly varies from the equator to the pole with a single peak in each hemisphere (green line in Fig. 3*D*). The changes in AHT_{SENS} and AHT_{RAD} both counteract those in AHT_{L_vE}. This is because the reduction in evaporation is compensated for by increases in the upward sensible and net radiative fluxes to balance the surface energy budget. Since these compensations are largest in the tropics, they result in poleward AHT_{SENS} and AHT_{RAD}.

The roles of evaporation in different regions can also be probed by additional experiments where evaporation is reduced only in the tropics (*SI Appendix*, Fig. S5 *B*, *E*, and *H*) or the extratropics (*SI Appendix*, Fig. S5 *C*, *F*, and *I*) separately. When evaporation is reduced only in the tropics, there is a global reduction in AHT_{TOTAL} driven by a change in AHT_{L_vE}. The change in AHT_{TOTAL} is similar to that of the global reduction in evaporation but with a sharp decrease in AHT_{L_vE} at 30°, which is compensated by AHT_{SENS} and AHT_{RAD}. This sharp decrease at 30° is likely a result of the sharp boundary created between the region with reduced evaporation and the region without. When evaporation is only reduced in the extratropics, there are small decreases in AHT_{TOTAL} due to increases in AHT_{L_vE} (associated with a stronger evaporation gradient across 30°) being compensated by decreases in AHT_{SENS} and AHT_{RAD}. Poleward of 50°, decreases in AHT_{TOTAL} closely match decreased AHT_{L_vE}, which suggest that a portion of AHT_{TOTAL} into the high latitudes is governed by extratropical evaporation. An interesting result of these experiments is that reductions in tropical evaporation alone nearly replicate the changes in AHT_{TOTAL} seen in the experiment with global evaporation reduction (c.f. the black lines in *SI Appendix*, Fig. S5 *G* and *H*), since the heat transport at the subtropical boundary transports latent heating from the Hadley cell further poleward (8, 26). In contrast, changes in extratropical evaporation have little consequence for tropical AHT_{TOTAL} because of the compensation of AHT_{SENS} and AHT_{RAD} in the tropics in that experiment. The exact nature of this compensation at the subtropical boundary remains a topic for future study.

A more extreme example of reduced evaporation resulting in reduced AHT_{TOTAL} comes from "Snowball Earth," e.g., Neoproterozoic climate states where ice covered the entirety of Earth's surface (39). We compare two aquaplanet simulations meant to simulate Neoproterozoic conditions, one which has only small ice caps and one which becomes an ice-covered snowball earth.[§] The simulation with icecaps has AHT similar to present day (Fig. 3*E*), while in the snowball earth conditions, AHT_{TOTAL} decreases drastically (Fig. 3*F*), as previously noted by refs. 40–42. The increased surface albedo of the snowball climate reflects more energy, leaving less for the surface fluxes (*SI Appendix*, Fig. S6), and as a consequence, AHT_{L_vE} decreases to about a tenth of its previous value. The small remaining AHT_{TOTAL} comes almost entirely from AHT_{SENS}. These results support our hypothesis; by greatly reducing the strength of the evaporation, AHT_{TOTAL} can no longer be maintained and thus greatly decreases. This happens despite the increase in baroclinicity seen in snowball

[§] Originally reported in ref. 30; see *Materials and Methods* for further details. The surface temperature and ice cover are shown in *SI Appendix*, Fig. S6*A*.

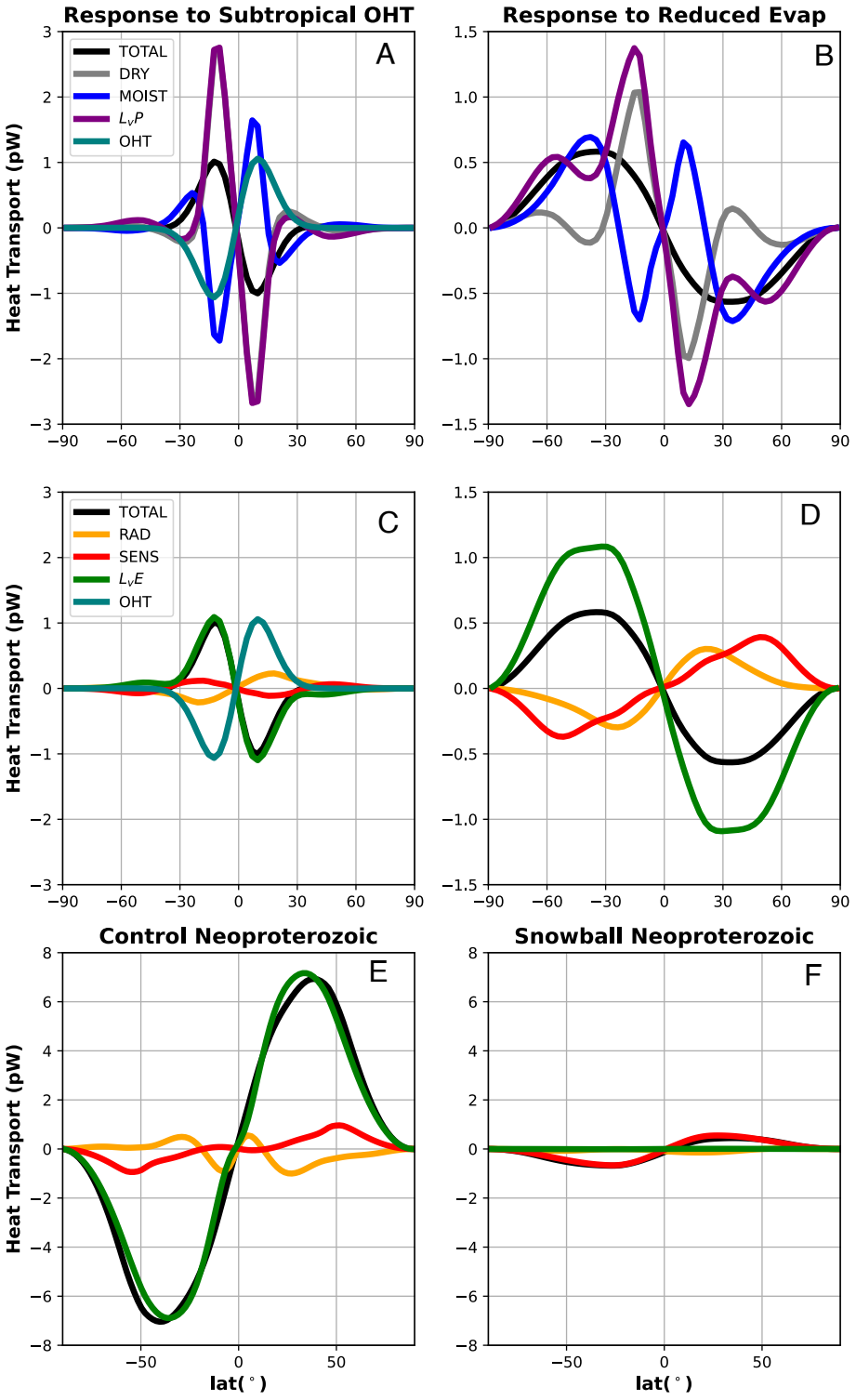

Fig. 3. Differences (e.g., the difference between the perturbed climate and the control shown in Fig. 2 *A* and *C*) in implied heat transports for the Aquaplanet with a subtropical Ocean Heat Transport applied experiment (*A* and *C*) with halved evaporation coefficient (*B* and *D*), showing the moist, dry decomposition and AHT_{L_vP} (*A* and *B*), and the MSE decomposition (*C* and *D*). The control Neoproterozoic heat transport (*E*) and the Snowball Neoproterozoic (*F*) from ref. 30 are also shown; see *Materials and Methods* for details.

earth climates (42), demonstrating the importance of the energy added by evaporation to maintaining AHT_{TOTAL}. While the snowball earth represents a climate state where the sensible fluxes are the dominant mechanism maintaining the AHT, the large decline in AHT compared to the control climate is due to the large decrease in evaporation.

D. The Atmospheric Heat Transport Response to CO_2 Is Mediated through Evaporation. Doubling CO_2 in the gray radiation aquaplanet model creates compensating AHT_{MOIST} and AHT_{DRY} responses in the tropics (Fig. 4*A*). The AHT_{DRY} is dominated by AHT_{L_vP} (Fig. 4*A*) however, so the compensation in the moist and dry components comes mostly from changes

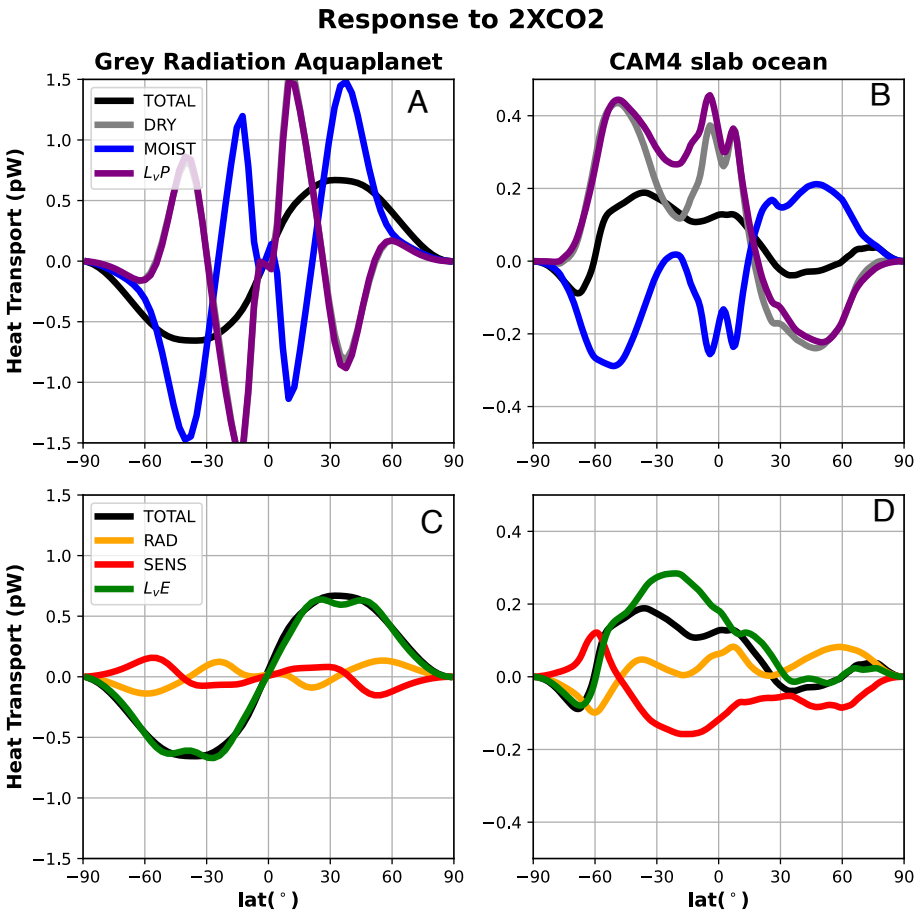

Fig. 4. Differences in implied heat transports for the gray radiation aquaplanet response to doubling CO_2, (*A* and *C*), and the CAM4 slab ocean response to doubling CO_2 (*B* and *D*), showing the moist, dry decomposition and AHT_{L_vP} (*A* and *B*), and the MSE decomposition (*C* and *D*). The CAM4 control heating rates and implied heat transports are shown in *SI Appendix*, Fig. S2. Note that AHT_{DRY} is not visible in *A* because it is covered by AHT_{L_vP}, which matches it closely.

in condensation. The total AHT_{TOTAL} increases poleward, and this increase is due almost entirely to AHT_{L_vE} with changes in AHT_{SENS} and AHT_{RAD} largely canceling (Fig. 4*C*). The changes in evaporation are largest in the tropics because of the Clausius–Clapeyron effect strengthening the equator-to-pole evaporation gradient. That is, AHT_{TOTAL} changes can be understood simply in terms of meridional gradients in evaporation as the climate warms, despite the complexity of compensations between AHT_{MOIST} and AHT_{DRY}. The enhanced evaporation is balanced by increased longwave cooling; however, since the longwave cooling has small meridional gradients, there is a large resulting AHT_{L_vE} transport to restore energetic balance.

Next, we compare these results to a fully parameterized atmospheric model attached to a slab ocean (CAM4¶). The AHT_{TOTAL} displays large compensations between AHT_{MOIST} and AHT_{DRY} Fig. 4*B*; similar results for slab ocean models were found in ref. 19. The compensating changes in AHT_{DRY} and AHT_{MOIST} result from enhanced precipitation moderating the tradeoff between AHT_{MOIST} and AHT_{DRY}, with the changes in the latter dominated by AHT_{L_vP}. In the framework introduced in this paper, AHT_{TOTAL} is largely dominated by AHT_{L_vE}, which removes the compensation between AHT_{MOIST} and AHT_{L_vP}. Unlike the gray radiation aquaplanet, the response to CO_2 doubling in CAM4 has a large hemispheric asymmetry, with a small increase in northward transport across the equator. This is caused by the change in surface shortwave flux over the Southern Ocean associated with cloud feedbacks operating in the CAM4 model, but not in the gray radiation model (*SI Appendix*, Fig. S8). Although the causes of evaporation differ between the gray radiation aquaplanet and CAM4, the response of AHT_{TOTAL} is largely caused by AHT_{L_vE} in both models.

Discussion and Conclusions

Our results show that the heat transport of the atmosphere is largely governed by the meridional distribution of surface evaporation in modern-day Earth-like climates. There are several simple perspectives that can explain why this is. From the perspective of Eq. **6**, evaporation governs AHT because the dominant terms in the energy budget are evaporation and radiative cooling, and since the meridional gradient of evaporation is much larger than the meridional gradients of radiative cooling, atmospheric heat transport is largely in balance with evaporation. From an atmospheric transport perspective, evaporation governs AHT because the AHT_{L_vE} combines the contributions of moisture transport and condensation ($AHT_{MOIST} + AHT_{L_vP} = AHT_{L_vE}$). This can be explained following an air parcel that starts in the boundary layer. The parcel will gain MSE from evaporation in the boundary layer, initially as water vapor. As the parcel travels through the atmosphere, this water vapor will be condensed, converting water vapor to DSE, which is eventually removed by radiative cooling. The initial transport of water vapor corresponds

¶Originally reported in ref. 43; see *Materials and Methods* for details. The climatology is shown in *SI Appendix*, Fig. S7.

to AHT_{MOIST}, the transport of DSE from condensation to AHT_{L_vP}, and the total transport of MSE governed by evaporation to AHT_{L_vE}.

From an atmospheric energy flow perspective, evaporation governs AHT because of the distribution of shortwave absorption in the climate system. The climate system absorbs shortwave radiation and emits longwave radiation. The combined AHT and OHT are set by meridional gradients in radiation at the Top of the atmosphere, but the partitioning between AHT and OHT is set by the surface energy budget. Globally, much of the shortwave energy is absorbed at the surface, but since most of the thermal radiation emitted at the top of the atmosphere originates from the atmosphere, most of the energy absorbed at the surface has to be transferred back to the atmosphere (24). Evaporation is one of the primary mechanisms for doing this, and since the Clausius–Clapeyron relation depends strongly on temperature, it has strong meridional gradients, which need to be balanced by AHT. This perspective is distinct from considering the total heat transport which is determined by the top of atmosphere radiation gradients, which are largely governed by the shortwave absorption, with minor compensations from gradients in outgoing longwave radiation (*SI Appendix*, Fig. S1*C*). The difference between the two is explained by surface absorption, which effectively converts shortwave energy into atmospheric latent energy via evaporation. In other words, evaporation governs AHT in modern-day climates because the surface absorbs more shortwave energy than the atmosphere and transfers that energy to the atmosphere as latent heat.

It is interesting to note that in the atmosphere, the implied AHT from shortwave absorption largely cancels with the implied AHT from longwave cooling (*SI Appendix*, Fig. S1*D*, equivalent to noting that the gradients in Q_{RAD} in Fig. 1*C* are small). Note that this is separate from considering the Top of atmosphere radiation gradients, which do not include this cancellation, *SI Appendix*, Fig. S1*C*). It is not obviously clear to us why this is the case; however, it is true not just of a single model or present-day observations, but true of a large array of models and perturbed climate experiments. Delving into this problem will likely uncover interesting new perspectives on atmospheric energetics.

Our analysis presents a contrasting perspective to the traditional perspective that AHT_{TOTAL} can be understood as the small residual between compensating AHT_{MOIST} and AHT_{DRY} transports resulting from different gradients in surface moisture and temperature (19, 44, 45), which roughly corresponds to the moist and dry perspective considered here. In particular, Held and Soden (19) show calculations similar to Fig. 4*B* and include the compensation between AHT_{DRY} and AHT_{MOIST} as an explicit parameter in their theory of AHT. We argue here that the compensation between AHT_{MOIST} and AHT_{DRY}—both in the climatological meridional distribution and in changes under climate forcing—is a consequence of precipitation mediating the hand-off between AHT_{MOIST} and AHT_{DRY} with no impact on AHT_{TOTAL}. The perspective obtained using AHT_{L_vE} is more useful for understanding AHT_{TOTAL} since it accounts for this hand-off; however, it does so at the expense of the ability to diagnose changes to AHT_{MOIST} alone, which is important for hydroclimate. We stress that this perspective does not make the traditional perspective incorrect but instead gives additional physical insight into the processes that govern atmospheric heat transport.

An interesting question to ask is whether the main result in this paper, that AHT_{TOTAL} is mostly determined by AHT_{L_vE}, would hold for climates different from modern-day Earth-like conditions. For small climate perturbations, the changes in evaporation and other terms in the energy budget are relatively small, with global evaporation changing at a rate of 2 to 3% per degree of global warming (46), and so AHT_{L_vE} will dominate AHT_{TOTAL} in these climate states. This includes future global warming scenarios (46), past warm paleoclimates such as the Pliocene (47), and past cold paleoclimates such as the Last Glacial Maximum (48). This range of applicability means that the perspective outlined in this paper will be useful for interpreting changes in AHT between modern-day Earth and the recent past and near future.

In the experiments shown here, there is a compensation between changes in AHT_{L_vE} and the dry processes AHT_{SENS} and AHT_{RAD} (e.g., the evaporation reduction experiments Fig. 3*D* and *SI Appendix*, Fig. S5), which act to reduce the changes in AHT_{TOTAL} from what would be expected through AHT_{L_vE} changes alone. This is an important observation because it explains why AHT_{TOTAL} does not match the evaporation changes in the reduced evaporation experiment, particularly in the tropics in the reduced extratropical evaporation experiment. However, this compensation cannot continue indefinitely; in the Snowball Earth experiments, the changes in AHT_{SENS} and AHT_{RAD} are not able to match the changes from AHT_{L_vE}, and there is a large decrease in AHT_{TOTAL}, since the absorbed shortwave radiation also greatly decreases. These observations represent one of the key limitations of our theory: in most climate perturbations, evaporation is not the only term in the surface energy budget that changes, which has the potential for compensating changes from dry processes. Studying the surface energy balance and AHT in climate states where evaporation is artificially depressed, or where evaporation is so limited that the heat transport is driven by sensible and radiative processes, are interesting topics for the future and may shed further light on the physics behind the dominant energy balance in the atmosphere of modern-day Earth.

Materials and Methods

The following datasets are used in this study:

1. The ERA5 reanalysis is created by taking a high-resolution forecasting model (nominal 31-km resolution), which is constrained using observations with a 12-h 4D-Var ensemble data assimilation (4). Here, we use data from 1979 to 2020. Since the reanalysis does not conserve water vapor or DSE, we remove a global mean of 0.83 W/m^2 from Q_{MOIST} and 4.57 W/m^2 from Q_{DRY}. The data are available from the ECMWF, e.g., https://cds.climate.copernicus.eu/#!/search?text=ERA5&type=dataset.
2. The Gray radiation aquaplanet is a spectral dynamic core, run at T42 resolution with 30 vertical levels, with several physical parameterizations, a "2+1" gray radiation scheme that includes a water vapor window and global CO_2 concentration parameter, a water vapor tracer that undergoes grid-scale condensation and subgrid-scale condensation, a boundary layer scheme with bulk surface fluxes (29). At the surface, there is a 10-m slab ocean surface, which does not move water but has prognostic temperatures. There is no land, sea ice, or clouds in the model. The model is run with a seasonal cycle. In the default configuration, the model is run with 370 ppm CO_2. The model is run with the "heat tagging" method of ref. 26. The data are available from https://doi.org/10.5281/zenodo.6626557.
3. The Northwestland is a very similar model to the gray radiation aquaplanet, but differs in two important ways: First, the radiation scheme is the default gray radiation scheme described in ref. 29, and second, it includes a land surface in the northwest quadrant; see ref. 31 for details. The control simulation without the land surface is shown in *SI Appendix*, Fig. S2, for comparison to Fig. 2. The data are available from https://datadryad.org/stash/dataset/doi:10.6078/D1399Q.

4. The NCAR CAM4 atmospheric model has a horizontal resolution of 0.9 × 1.25° and 26 vertical levels and has full radiation, deep and shallow convection, boundary layer, and cloud parameterizations. The configurations used here are coupled to a slab ocean forced with a spatially heterogeneous monthly climatology of ocean heat flux convergence derived from a fully coupled preindustrial control simulation, see ref. 43 for further details. The AHT in the control simulation in shown in *SI Appendix*, Fig. S5, for comparison to Fig. 1. The data are available from https://doi.org/10.5281/zenodo.3735441.
5. The Neoproterozoic Aquaplanet simulations use the ICON-A Climate model, run in a slab aquaplanet configuration with a nominal horizontal resolution of 160 km and a solar constant of 1,285 W/m^2 to represent the weaker Neoproterozoic sun; see ref. 30 for further details. The control and Snowball Earth simulations corresponds to the "Winton" sea ice model simulations with 3,000 ppmv and 1,875 ppmv CO_2 simulations, respectively. For reference, *SI Appendix*, Fig. S4*A* shows the control and snowball surface temperature and sea ice fields. The data are available from https://gitlab.phaidra.org/climate/hoerner-seaice-james-2022.

Data, Materials, and Software Availability. Gray Radiation Model Output data have been deposited in Zenodo (https://doi.org/10.5281/zenodo.6626557) (49).

ACKNOWLEDGMENTS. R.F. was supported by the NOAA Climate and Global Change Postdoctoral Fellowship programs for the Advancement of Earth System Science (CPAESS) under award NA18NWS4620043B. R.F. thanks Lily Hahn for the CAM4 Slab Ocean data and Johannes Hörner for the Neoproterozoic Aquaplanet data, and R.F. and S.R. thank Marysa Laguë for the Northwestland data. K.C.A. and A.D. acknowledge support from NSF Award CLD-2019647. K.C.A. and S.R. acknowledge support from NSF Award OCE-1850900. Original simulations in this paper were performed on the Niagara supercomputer at the SciNet HPC Consortium.

Author affiliations: [a]Department of Atmospheric Sciences, University of Washington, Seattle, WA 98195; [b]Polar Science Center, Applied Physics Laboratory, University of Washington, Seattle, WA 98105; [c]School of Oceanography, University of Washington, Seattle, WA 98195; and [d]Department of Physics, University of Toronto, Toronto, ON M5S 1A1, Canada

1. R. Pierrehumbert, *Principles of Planetary Change* (Cambridge University Press, 2010).
2. J. Ling, C. Zhang, Diabatic heating profiles in recent global reanalyses. *J. Clim.* **26**, 3307–3325 (2013).
3. K. C. Armour, N. Siler, A. Donohoe, G. H. Roe, Meridional atmospheric heat transport constrained by energetics and mediated by large-scale diffusion. *J. Clim.* **32**, 3655–3680 (2019).
4. H. Hersbach *et al*., The era5 global reanalysis. *Q. J. R. Meteorol. Soc.* **146**, 1999–2049 (2020).
5. M. Newman, G. N. Kiladis, K. M. Weickmann, F. M. Ralph, P. D. Sardeshmukh, Relative contributions of synoptic and low-frequency eddies to time-mean atmospheric moisture transport, including the role of atmospheric rivers. *J. Clim.* **25**, 7341–7361 (2012).
6. T. A. Shaw, O. Pauluis, Tropical and subtropical meridional latent heat transports by disturbances to the zonal mean and their role in the general circulation. *J. Atmos. Sci.* **69**, 1872–1889 (2012).
7. P. Stone, Constraints on dynamical transports of energy on a spherical planet. *Dyn. Atmos. Oceans* **2**, 123–139 (1978).
8. K. E. Trenberth, D. P. Stepaniak, Seamless poleward atmospheric energy transports and implications for the Hadley circulation. *J. Clim.* **16**, 3706–3722 (2003).
9. J. P. Peixoto, A. H. Oort, *Physics of Climate* (American Institute of Physics, New York, NY, 1992).
10. K. E. Trenberth, A. Solomon, The global heat balance: Heat transports in the atmosphere and ocean. *Clim. Dyn.* **10**, 107–134 (1994).
11. O. Pauluis, A. Czaja, R. Korty, The global atmospheric circulation in moist isentropic coordinates. *J. Clim.* **23**, 3077–3093 (2010).
12. R. Caballero, P. L. Langen, The dynamic range of poleward energy transport in an atmospheric general circulation model. *Geophys. Res. Lett.* **32** (2005).
13. D. M. Frierson, I. M. Held, P. Zurita-Gotor, A gray-radiation aquaplanet moist GCM. Part II: Energy transports in altered climates. *J. Atmos. Sci.* **64**, 1680–1693 (2007).
14. P. A. O'Gorman, T. Schneider, The hydrological cycle over a wide range of climates simulated with an idealized GCM. *J. Clim.* **21**, 3815–3832 (2008).
15. M. A. Knietzsch, A. Schröder, V. Lucarini, F. Lunkeit, The impact of oceanic heat transport on the atmospheric circulation. *Earth Syst. Dyn.* **6**, 591–615 (2015).
16. H. Yang, Q. Li, K. Wang, Y. Sun, D. Sun, Decomposing the meridional heat transport in the climate system. *Clim. Dyn.* **44**, 2751–2768 (2015).
17. N. Siler, G. H. Roe, K. C. Armour, Insights into the zonal-mean response of the hydrologic cycle to global warming from a diffusive energy balance model. *J. Clim.* **31**, 7481–7493 (2018).
18. A. Donohoe, K. C. Armour, G. H. Roe, D. S. Battisti, L. Hahn, The partitioning of meridional heat transport from the last glacial maximum to CO_2 quadrupling in coupled climate models. *J. Clim.* **33**, 4141–4165 (2020).
19. I. M. Held, B. J. Soden, Robust responses of the hydrological cycle to global warming. *J. Clim.* **19**, 5686–5699 (2006).
20. Y. Wu, O. Pauluis, Examination of isentropic circulation response to a doubling of carbon dioxide using statistical transformed Eulerian mean. *J. Atmos. Sci.* **70**, 1649–1667 (2013).
21. N. Fischer, J. Jungclaus, Effects of orbital forcing on atmosphere and ocean heat transports in Holocene and Eemian climate simulations with a comprehensive earth system model. *Clim. Past* **6**, 155–168 (2010).
22. R. D. Russotto, T. P. Ackerman, Energy transport, polar amplification, and ITCZ shifts in the GeoMIP G1 ensemble. *Atmos. Chem. Phys.* **18**, 2287–2305 (2018).
23. K. E. Trenberth, D. P. Stepaniak, Covariability of components of poleward atmospheric energy transports on seasonal and interannual timescales. *J. Clim.* **16**, 3691–3705 (2003).
24. K. E. Trenberth, D. P. Stepaniak, The flow of energy through the earth's climate system. *Q. J. R. Meteorol. Soc.* 130, 2677–2701 (2004).
25. A. Numaguti, Dynamics and energy balance of the Hadley circulation and the tropical precipitation zones: Significance of the distribution of evaporation. *J. Atmos. Sci.* **50**, 1874–1887 (1993).
26. R. Fajber, P. J. Kushner, Using "heat tagging" to understand the remote influence of atmospheric diabatic heating through long-range transport. *J. Atmos. Sci.* **78**, 2161–2176 (2021).
27. L. Gimeno, R. Nieto, A. Drumond, A. M. Durán-Quesada, "Ocean evaporation and precipitation" in *Earth System Monitoring* (Springer, 2013), pp. 291–318.
28. R. Zhang, X. Wang, C. Wang, On the simulations of global oceanic latent heat flux in the CMIP5 multimodel ensemble. *J. Clim.* **31**, 7111–7128 (2018).
29. G. K. Vallis *et al*., Isca, v1.0: A framework for the global modelling of the atmospheres of Earth and other planets at varying levels of complexity. *Geosci. Mod. Dev.* **11**, 843–859 (2018).
30. J. Hörner, A. Voigt, C. Braun, Snowball earth initiation and the thermodynamics of sea ice. *J. Adv. Mod. Earth Syst.* **14**, e2021MS002734 (2022).
31. M. M. Laguë, M. Pietschnig, S. Ragen, T. A. Smith, D. S. Battisti, Terrestrial evaporation and global climate: Lessons from Northland, a planet with a hemispheric continent. *J. Clim.* **34**, 2253–2276 (2021).
32. J. Marshall, A. Donohoe, D. Ferreira, D. McGee, The ocean's role in setting the mean position of the inter-tropical convergence zone. *Clim. Dyn.* **42**, 1967–1979 (2014).
33. C. Herweijer, R. Seager, M. Winton, A. Clement, Why ocean heat transport warms the global mean climate. *Tellus A: Dyn. Meteorol. Oceanog.* **57**, 662–675 (2005).
34. H. Singh, N. Feldl, J. E. Kay, A. L. Morrison, Climate sensitivity is sensitive to changes in ocean heat transport. *J. Clim.* **35**, 2653–2674 (2022).
35. I. M. Held, The partitioning of the poleward energy transport between the tropical ocean and atmosphere. *J. Atmos. Sci.* **58**, 943–948 (2001).
36. A. Czaja, J. Marshall, The partitioning of poleward heat transport between the atmosphere and ocean. *J. Atmos. Sci.* **63**, 1498–1511 (2006).
37. X. J. Levine, T. Schneider, Response of the Hadley circulation to climate change in an aquaplanet GCM coupled to a simple representation of ocean heat transport. *J. Atmos. Sci.* **68**, 769–783 (2011).
38. S. M. Kang, Y. Shin, F. Codron, The partitioning of poleward energy transport response between the atmosphere and Ekman flux to prescribed surface forcing in a simplified GCM. *Geosci. Lett.* **5**, 1–10 (2018).
39. R. Pierrehumbert, D. Abbot, A. Voigt, D. Koll, Climate of the neoproterozoic. *Annu. Rev. Earth Planet. Sci.* **39**, 417–460 (2011).
40. R. T. Pierrehumbert, Climate dynamics of a hard snowball earth. *J. Geophys. Res.: Atmos.* **110** (2005).
41. M. Brunetti, J. Kasparian, C. Vérard, Co-existing climate attractors in a coupled aquaplanet. *Clim. Dyn.* **53**, 6293–6308 (2019).
42. T. A. Shaw, R. J. Graham, Hydrological cycle changes explain weak snowball earth storm track despite increased surface baroclinicity. *Geophys. Res. Lett.* **47**, e2020GL089866 (2020).
43. L. C. Hahn *et al*., Antarctic elevation drives hemispheric asymmetry in polar lapse rate climatology and feedback. *Geophys. Res. Lett.* **47**, e2020GL088965 (2020).
44. G. K. Vallis, R. Farneti, Meridional energy transport in the coupled atmosphere–ocean system: Scaling and numerical experiments. *Q. J. R. Meteorol. Soc.* **135**, 1643–1660 (2009).
45. T. A. Shaw, A. Voigt, What can moist thermodynamics tell us about circulation shifts in response to uniform warming? *Geophys. Res. Lett.* **43**, 4566–4575 (2016).
46. R. P. Allan *et al*., Advances in understanding large-scale responses of the water cycle to climate change. *Ann. N. Y. Acad. Sci.* **1472**, 49–75 (2020).
47. N. J. Burls, A. V. Fedorov, Wetter subtropics in a warmer world: Contrasting past and future hydrological cycles. *Proc. Natl. Acad. Sci. U.S.A.* **114**, 12888–12893 (2017).
48. W. R. Boos, Thermodynamic scaling of the hydrological cycle of the last glacial maximum. *J. Clim.* **25**, 992–1006 (2012).
49. R. Fajber, Heat Tagging Data For Idealized Isca Aquaplanets. *Zenodo*. https://doi.org/10.5281/zenodo.6626557. Deposited 9 June 2022.